Modeled tracheidograms disclose drought influence on *Pinus sylvestris* tree-rings structure from Siberian forest-steppe

Margarita I. Popkova[1,*], Eugene A. Vaganov[1,2], Vladimir V. Shishov[1,3], Elena A. Babushkina[4], Sergio Rossi[5], Marina V. Fonti[1], Patrick Fonti[6]

[1] Siberian Federal University, Krasnoyarsk, Russia

[2] V.N. Sukachev Institute of Forest SB RAS, Krasnoyarsk, Russia

[3] Le Studium Loire Valley Institute for Advanced Studies, Orléans, France

[4] Khakassian Technical Institute, Siberian Federal University, Abakan, Russia

[5] Département des Sciences Fondamentales, Université du Québec à Chicoutimi, Chicoutimi, QC, Canada

[6] WSL Swiss Federal Research Institute, Landscape Dynamics, Birmensdorf, Switzerland

*** Correspondence:**
Patrick Fonti
patrick.fonti@wsl.ch

Total word count: 4313 words

Number of Figures: 5 (all in color)

Number of Tables: 2

Supporting Figures: 3

Keywords: cambial activity, cell size, process-based Vaganov-Shashkin model, South Siberia, tracheid, tracheidogram, VS-oscilloscope

Abstract

Wood formation allows trees to adjust in a changing climate. Understanding what determine its adjustment is crucial to evaluate impacts of climatic changes on trees and forests growth. Despite efforts to characterize wood formation, little is known on its impact on the xylem cellular structure. In this study we apply the Vaganov-Shashkin model to generate synthetic tracheidograms and verify its use to investigate the formation of IADFs, one of the most frequent climate tree-ring markers in drought-exposed sites. Results indicate that the model can produce realistic tracheidograms, except for narrow rings (<1 mm), when cambial activity stops due to an excess of drought or a lack of growth vigor. These observations suggest that IADFs are caused by a release of drought limitation to cells formation in the first half of the growing season, but that narrow rings are indicators of an even more extreme and persistent water stress. Taking the example of IADFs formation, this study demonstrated that the Vaganov-Shashkin model is a useful tool to study the climatic impact on tree-ring structures. The ability to produce synthetic tracheidogram represents an unavoidable step to link climate to tree growth and xylem functioning under future scenarios.

1 Introduction

As long-living and sessile organisms, wooden plants needs to continuously adjust their structure to survive under changing environmental conditions. These adjustments are usually achieved while growing (Meinzer *et al.*, 2011). Thanks to the primary and secondary meristems, plants are indeed constantly producing new tissues when conditions are favorable (Vaganov *et al.*, 2006). The cambium can modify the number of cells produced, and their morphological characteristics to regulate the important xylem and phloem functions of transport, storage and mechanical support. In this way, not only the tissues are constantly renewed, but also their form and functioning. This capacity offers trees the necessary dynamic to face changes. However, since wood formation requires resources and time to take place (Steppe *et al.*, 2015), the current environment conditions strongly influence the width, structure and chemical composition of the annual rings, thus limiting the ability of plants to acclimate and endure. These limitations can restrict the physiology over several years, as already observed as a consequence of increasing drought pressure (Anderegg *et al.*, 2013; Britez *et al.*, 2014), threatening plant survival (McDowell *et al.*, 2008) and eventually leading to forest mortality (Allen *et al.*, 2010).

A better understanding of the chain between environment, tree-physiology, wood formation, wood structure and plant performance is unavoidable to soundly assess the fate of trees species and provenances under a rapidly changing environment (Sass-Klaassen *et al.*, 2016). Without a clear long-term and high-resolved perspective of the process of xylem formation and its interaction with the environment, it is not possible to fully comprehend how annual growth rings and their typical wood structures are formed and respond to climate and their extreme events (Pacheco *et al.*, 2016; Rathgeber *et al.*, 2016). Evidences of the impact of the environment on plant growth are not only manifold, but are also exploited to reconstruct past environmental conditions via the study of tree-rings (Fritts, 1976). Novel methods over the last decades have extended interests into the processes of tree-ring formation towards higher intra-annual resolution and deeper mechanistic understanding of environmental impact (McCarroll & Loader, 2004; Fonti *et al.*, 2010). Attention has also been given to the process of xylogenesis (e.g., Cuny *et al.*, 2015) to better assess cambial phenology (e.g., Rossi *et al.*, 2016), timing (Carrer *et al.*, 2017) and dynamic (Cuny *et al.*, 2014) of growth. Based on the improved spatial (cellular) and temporal (weekly) resolution, it has now become possible to better

link the impact of specific environmental events to the processes shaping the amount of carbon fixed (Cuny *et al.*, 2015) and its cellular structure (e.g., Abrantes *et al.*, 2013; Castagneri *et al.*, 2015), as well as its influences on the functioning of the xylem (e.g., Mayr *et al.*, 2006; Martin-Benito *et al.*, 2017).

Intra-annual density fluctuations (IADF), i.e., a density anomaly appearing within the annual ring due to the occurrence of latewood-like cells within earlywood, or earlywood-like cells within latewood, represent one of the most obvious examples of climatic impact on the tree-ring structure (Fritts, 1976). IADFs are in general associated to unusual strong events (as drought or cold period) changing the "typical" process of cell development" as e.g.; a temporary decrease in growth rate. Its occurrence has been suggested to be associated with plastic adjustments to maintain the balance between hydraulic efficiency and safety under short-term variations in environmental conditions (De Micco *et al.*, 2016). Despite numerous investigations (e.g., Nabais *et al.*, 2014;), reliability of IADFs occurrence and distribution is still uncertain (Campelo *et al.*, 2015). IADFs do not arise in all the trees within the same site, not even all drought events trigger IADFs. This variability has been associated to differences in sensitivity among species (Pacheco *et al.*, 2016), tree size and age (Campelo *et al.*, 2015), growth rate (Rigling *et al.*, 2001), sex (Olivar *et al.*, 2015), or to difference in intensity and duration of the climatic event (Vieira *et al.*, 2017).

To better assess the ability of tree species to acclimate and endure a changing environment requires tools allowing projecting growth under future climatic scenarios (Guiot *et al.*, 2014). Process-based models of tree-ring growth (e.g., *MuSICA* (Ogee *et al.*, 2003); *CASSIA* (Schiestl-Aalto *et al.*, 2015); and *CASTANEA* (Delpierre *et al.*, 2012)) provide this additional perspective for simulating intra-annual growth under differing climatic scenario as increasing intensity and duration of drought (e.g.; Wilkinson *et al.*, 2015). Several process-based model exists to estimate the annual course of wood biomass, which is essential to study the impact of intra-seasonal climatic event on tree-growth. However, these models are usually not able to provide data on the formed wood structure (with few exception as Deleuze & Houllier (1998) and *CAMBIUM* model by Downes *et al.*, (2009)) – one of the most critical connections between environment and plant functioning – precluding the opportunity to connect structure to function. The Vaganov-Shashkin model (*VS-model*, Vaganov *et al.*, 2006) is an environmental driven conifer tree-ring growth model that has proven to provide reliable estimates under strong limited conditions (for examples of model applications see (Touchan *et al.*, 2012; Shishov *et al.*, 2016). A singularity of this model is the assumption that the environment (via the most limiting environmental factor) is determining xylem cell differentiation (cell enlargement and wall thickening) only during the time-window the cells are residing in the cambial zone. In this way, the model computes daily growth rate relative to the growth in absence of limitations. To run, the model only requires daily temperature and precipitation data and needs to be calibrated to the growth characteristics for the selected species specific to the site considered (Vaganov *et al.*, 2006; Shishov *et al.*, 2016).

2 Materials and Methods

2.1 Study site and climate

This study uses wood cores collected in late 2013 on a foothill-forested site around Malaya Minusa (53°43′ N, 91°47′ E, 251 m a.s.l.), southern Siberia (Russia), a village close to Minusinsk at the border with the Altai–Sayan region. The area is a steppe-like landscape characterized by a cold and semi-arid climate. Records from the 25 km close meteorological station of Minusinsk (53°41' N,

91°40' E, 254 m a.s.l.) indicated an average annual temperature of 1.0°C and precipitation sum of 341 mm (average 1936-2013), 90% of which falls from the end of April to the beginning of October. The site is composed of a mixed forest of birch (*Betula pendula*) and pine (*Pinus sylvestris*) growing on deep sandy soil covered by sedge-grass and mosses.

2.2 Tree-ring width and tracheidograms

The wood cores were collected from a selection of 20 damage-free, dominant and mature *Pinus sylvestris* trees. Two parallel radial cores were extracted at stem breast height from each tree using an increment borer with a diameter of 5 mm. Half of the cores (one per tree) were prepared to build an annual growth chronology– necessary to calibrate the VS-model – and the second half served the description of the tracheid anatomical properties. Ring widths were measured with a precision of 0.01 mm using a LINTAB measuring table connected to the TSAP software (Rinntech, Heidelberg, Germany). The obtained time-series were visually cross-dated and verified with the software *COFECHA* (Grissino-Mayer, 2001). A 50%-variance cubic smoothing spline with a 2/3 cut-off was used to remove non-climatic factors and the auto-correlations removed with an auto-regressive modeling. The residual tree-ring chronology (1936-2013) was finally obtained by averaging the individual time-series with a bi-weight robust mean (Cook & Kairiukstis, 1990).

Tracheidograms were built to characterize the variation of tracheid radial size along the annual rings (Vaganov, 1990). The cores from the five trees best correlating with the chronology ($R > 0.70$) were selected. Cell measurements were performed on cross-section images of safranin-stained micro-sections (15–20 µm thick) cut with a sliding microtome (Reichert, Germany) along the 50 last annual rings (1964 to 2013). The images were captured at a 400× magnification with a digital camera (5 Megapixels) connected to a microscope (Axio Imager A1m, Carl Zeiss, Germany). Tracheids radial cell diameter (TD) were assessed by measuring the lumen radial diameter (LD) and double tangential cell wall thickness (2CWT) along five undisturbed and representative radial files in each ring (Vaganov *et al.*, 2006; Seo *et al.*, 2014) using the image analysis package *Lineyka*, *SuperMoment* and *ProcessorKR* (Silkin, 2010). All measured files were standardized, i.e. adjusted to the rounded average cell number for the trees in that year (Vaganov *et al.*, 1985; Campelo *et al.*, 2016).

To perform analysis, from the 50 available calendar years, we selected three groups of years inducing specific tree-ring anatomical patterns (ring types), namely the narrow (N, 1965, 1974, 1983, 1998, 2012), wide (W, 1970, 1982, 1995, 2003, 2006) and IADF (I, 1969, 1992, 1999, 2007, 2013) rings. The selection of narrow and wide ring was based on the five years in the chronology with respectively the largest and smallest ring width (see Figure 1). The IADF have been based on the presence of IADF from the latewood type L+ (Campelo *et al.*, 2007), i.e. density fluctuation occurring in the latewood. These patterns have been identified using the tracheidograms and specifically when tracheid radial size in the second half of the ring showed an increase of > 10% compared to a previous local minima (Figure 2C).

2.3 Xylogenesis and tracheid anatomical measurements

To monitor seasonal tree-ring growth, microcores from 15 trees were collected at the stem breast height from April to October 2013 (with approx. a 10-days interval for a total of 18 sampling dates). Samples were fixed in water-glycerin-ethanol solution (1:1:1) to maintain the soft tissue in their original hydrated status. Cross-sections (15-µm thick) were obtained with a sliding microtome (Thermo Fisher Scientific HM 450), stained with safranin (1% solution) and astra blue (2% solution) and placed into glycerin on a microscope slide. Growth was assessed by counting along three radial

files the tracheids in the cambial, enlargement, wall thickening, and mature zone. The last collected micro-sections were used to characterize tracheid anatomy, by measuring the radial lumen size and the double cell wall thickness along five radial files using AxioVision (SE64 Rel. 4.9.1, Carl Zeiss, Jena, Germany).

2.4 VS-model calibration and assessment of daily growth rates

The VS-model computes relative daily growth rate (Gr) from daily data of temperature, precipitation and hours of sunlight. These computations require the calibration of the most sensitive parameters to the growing characteristics of the species at the site (Tychkov *et al.*, in review). We performed the model calibration (1960-2013) and verification (1934-1959) by comparing the simulated time series of annual growth rates with the site-specific detrended tree-ring width chronology using the VS-oscilloscope (Shishov *et al.*, 2016). This tool is specifically designed to interactively adjust the model parameters and directly visualize and assess the match between the model output and the indexed tree-ring width chronology. As input for the model we used the daily temperature and precipitation data from the meteorological station of Minusinsk (53°41' N, 91°40' E, 254 m a.s.l.) from January 1934 to December 2013.

2.5 Modeling tracheidogram for each grouping of radial patterns

The previously quantified associations have subsequently been applied to each ring type (N, W, and I) to assess the ability of the model to reproduce the expected pattern of the tracheidogram. Specifically, we run the model with the same original parameterization to first calculated the typical seasonal growth rates for each group and subsequently we applied the exponential dependency between growth rate and tracheid size to obtain the synthetic tracheidograms. As model input we first calculated and then smoothed with a loess function (span = 0.3) the daily temperature and precipitation average over the 5 calendar years included in each ring type. In order to account for the soil moisture legacy, the model was run on a sequence of three years, whereby the two first years where feed with the overall daily climate average (1936-2013) and the third year with the group average. Only the output relative to the third year has been considered for further analysis.

2.6 Linking growth rates to tracheid radial diameter

An important model assumption is that the main environmental conditions (temperature, light and soil moisture) occurring when the cells are residing in the cambial zone determine the (future) growth rate (Vaganov *et al.*, 2006). In other words, the growth rate of the cambial zone cells, i.e. the actively dividing cells, cannot be higher then allowed by the most limiting factor. To assign the average cell growth rates necessary to produce the tracheidograms, in this study we make the additional assumptions that i) the number of dividing cells over a full growing season corresponds to the number of cells produced in the tree ring, and ii) the actively dividing cells are successively produced with no overlap. Thus, we assigned the growth rate matching each dividing cell by calculating the average growth rates over the time period required to form the corresponding part of the tree-ring (Figure 3B). A corresponding R-code for time-assignment (VS-timing) has been developed for that purpose and applied to derive the linear dependency between the average cell growth rate and the tracheid size (Figure 3C-D). This relation is then inversely applied to estimate tracheid size (TD) from the growth rate obtained from the model.

2.7 Identifying threshold conditions inducing IADF

To identify the threshold conditions generating IADFs, we compared modeled tracheidograms from newly generated climatic scenarios obtained by progressively increasing the limitation of the main factor inducing the formation of IADF (i.e. by reducing precipitation by step of 20%). The same temperature course (as the average temperature among the groups) has been applied for each scenario to focus on the influence of precipitations only. The occurrence of IADF in the modeled tracheidograms has then been assessed with the same criteria used to its identification (Figure 2B).

3 Results

3.1 Trees and tree-ring characteristics

The selected *Pinus sylvestris* trees were on average 17.8 (± 1.4 sd) m tall and their stem DBH varied between 26 and 46 cm. Tree age ranged from 76 to 111 and their average annual radial growth (TRW) over the period 1936 to 2013 was 1.46 cm (Table 1). The common signal, expressed as the mean correlation among the individual detrended time series, was 0.62. The 5 trees selected for the tracheidograms were highly synchronized with the site chronology ($r = 0.77$) and showed a similar average annual growth of 1.33 cm. In terms of number of cell production, the annual increment was composed on average by 38 radially aligned tracheids per ring (from a minimum of 9 to a maximum of 76), but with variation among the trees (mean ranging from 21 to 49 tracheids).

3.2 Model calibration and verification

The model has been calibrated over the period 1960 to 2013 and verified (from 1936 to 1959) by comparing the time-series of the modeled cumulated annual growth rates with the detrended residual site chronology using the VS-oscilloscope (Vaganov *et al.*, 2006). The selected parameters are shown in Table 2. The calibrated model provided a simulated chronology matching the residual tree-ring chronology with a correlation of $r = 0.71$ ($p < 0.001$; $n = 54$ years) and a Gleichläufigkeit Glk of 80% over the calibration period, and a correlation of $r = 0.55$ ($p<0.001$, $n = 25$, Glk = 71%) for the validation one (Figure 1).

According to the model, the growing season at the site extended on average for 131 days ± 12, from DOY 137 ± 10 (May 18th) to DOY 268 ± 8 (September 26th). Growth was limited by drought from DOY 139 ± 10 (May 20th) to DOY 259 ± 10 (September 17th), and only affected by temperature limitation at both edges (beginning and end) of the growing season.

3.3 Tracheid anatomy and tracheidograms

The average tracheid radial diameter (TD) in the ring differed among trees ranging from 18.7 to 45.5 µm (Table 1). Intra-annually, TD usually decreased monotonically from a maximum in the earlywood (~ 60 µm) to a minimum in the latewood (~10 µm, Figure 2A), but in some cases it was possible to identify the typical signature of latewood IADF (Figure 2B). IADFs occurred mainly in particular years (i.e., 1973, 1995, 2001, 2007, 2009) and mostly when the ring width was > 1 mm (Figure 2C). The frequency of IADF occurrence was 21.2% (53 rings out of 250) and varied quite strongly among the trees (from 6% in D5 to 46% in D7).

3.4 Calculation of timing and growth rate of cambial cells

One assumption of the model is that the conditions occurring at time of formation of cambial cells determine their cell developmental stages. The correlation between the observed and modeled growth

rate of cambial division is r = 0.93 and r = 0.84 for the cambial and enlarging cells, respectively (Figure 3A,B). We used this assumption to first assign a time to each dividing cambial cell to subsequently assign the corresponding cumulative growth rate (Gr, Figure 3B). As shown in Figure 3C and Figure S1, there is a strong relationship between average cambial growth rate and tracheid radial diameter. The correlation distribution shows a high frequency of high correlation (Figure 3D). However, this relationship clearly weakens in some rings. However, in these specific rings, if the modeled growing season is progressively reduced, the correlations and the R^2 are considerably recovered (see Figure S2, S3).

3.5 Modeling and simulating growth rates and tracheidograms by ring type

The model calculations of the daily growth rates using the average daily climatic condition of the years of the narrow (N), wide (W) and IADF (I) ring types indicated a common decreasing growth rates between 37% (W) to 64% (N) during the first half of the growing season (up to DOY 210, Figure 4). During this period, the rates were about 42 and 48% higher for the wide ring then for the other two groups. The pattern among the groups differed in particular in the second part of the season, where the Grs continued to decrease in the wide rings, while it showed a substantial recovery before a new decrease at the end of the growing season for both IADF (+ 134%) and the narrow rings (+ 24%). Up to the ending of the growing season (i.e., from DOY 1 to 270) the precipitation sum was 394, 363 and 286 mm for W, I and N respectively, whereby the precipitation in the IADF group were initially not substantially differing from the narrow rings, but showed a strong increase in the second part of the growing season. Over the growing season (DOY 142 to 270), the average temperature among the groups ranged between 16.35 °C and of 16.64 °C.

The assessment of tracheid size (and thus of the average tracheidogram) for each group of year (using the average relationship obtained based on the observation, Figure 3) indicated that the model is able to reproduce the main pattern of the original tracheidogram, with presence of IADF only in the corresponding group (Figure 4C). However, the model failed to reproduce short rings, since growth rate, similarly to the IADF group, also recovered after the summer drought. A stop of growth induced at the end of the drought period would however provide a short ring, without IADF.

Model simulations performed to identify which conditions generate IADF by progressively reducing precipitation (by step of 20%) from W to I and I to N during the firs half of the growing season (period DOY 1 to 186) indicated that IADF started to appear when precipitations are below 132 mm only if the second part of the growing season get sufficient precipitations (199 mm, see scenario W80 in Figure 5). Notably, if the second part of the growing season persists with below average precipitation, the model predicts the formation of a narrow ring.

4 Discussion

To The application of the VS-model performed in this study, although based on assumptions simplifying the process of xylogenesis, provided outputs matching site observations. It is known that, differently to our assumptions, the xylem cells resulting from cambial zone are disposed in a radial band and thus successively undergo the differentiation program with some time overlap (Rathgeber *et al.*, 2016). Moreover, a latewood tracheid differentiation can easily last for more than a month (e.g.; (Cuny *et al.*, 2013) and consequently cambial division stops earlier then assumed in this study. Despite these assumptions, the VS-model provided i) time-series of annual growth rate well matching the site tree-ring chronology, ii) timing of cambial cells growth rates that matched with the observations of tissue formation performed in the field in 2013 (Figure 3A,B), and iii) modeled

tracheidograms reproducing most of the anatomical patterns of tree-rings typical in summer-drought exposed sites.

These results confirm the ability of the VS-model to deliver reliable annual growth outputs at cold and drought limited forest sites (Breitenmoser *et al.*, 2014), as in the Quilian Mountains and Tibetan Plateau (e.g.; (Zhang *et al.*, 2016; He *et al.*, 2017; Yang *et al.*, 2017), at the semi-arid central China (Shi *et al.*, 2016), or within the drought sensitive Mediterranean Basin (Touchan *et al.*, 2012). At our site, growth rates are generally limited by soil water shortage except for the margin of the growing season which are limited by cold (Arzac *et al.*, in review; Tychkov *et al.*, in review), as confirmed by results of climate-growth responses performed for the same species within the South-Central Siberian forest-steppe (Babushkina *et al.*, 2015). Newly, we could verify that the VS-model also provided convincing intra-annual output typical of summer drought-limited environments characterized by a bi-modal growth (e.g. (Camarero *et al.*, 2010; Pasho *et al.*, 2012; Vieira *et al.*, 2014) and a radial ring pattern with the occurrence of numerous IADF (e.g.; Campelo *et al.*, 2007; De Micco *et al.*, 2016; Zalloni *et al.*, 2016). On the one hand, the growth rates modeled for the 2013 growing season were synchronous in timing and proportion with the number of cambial and enlarging cells observed on micro-cores collected in the field ($r = 0.93$ and 0.84 for cambial and enlarging, respectively), including direct observations on five trees performed in the same area during the years 1979-1981 (Vaganov *et al.*, 1985). On the other hand, the tracheidograms simulated for the three ring types provided the expected radial patterns, with the occurrence of IADF in the second part of the annual ring for the IADF group.

However, interestingly, the model failed to reproduce the tracheid pattern of narrow rings by instead providing narrow rings with the occurrence of IADF. Strong indications suggest that this discrepancy is caused by a summer drought-induced growth stop in that particular year that the model misses to identify. In this specific case, there are indications that in extreme drought years, trees with reduced growth rate are not able to resume growth along with the drought release occurring in the second part of the season due to an excessive water shortage. This result is confirmed by previous observations indicating that water availability has a strong influence on growth rates and can induce an early cessation of wood formation (Eilmann *et al.*, 2009; Vieira *et al.*, 2017). Studies on IADF occurrence have already highlighted that IADFs were more frequent in younger trees (Vieira *et al.*, 2009; Battipaglia *et al.*, 2010) or in wider tree rings (Rigling *et al.*, 2001; Campelo *et al.*, 2013), supporting our suggestion that trees with smaller growth rates do not resume cambial division and thus do not form IADFs. The substantial improvement of the correlations and R^2 between cambial cell growth rates and cell diameter obtained when reducing the modeled growing season length (Figure S2 and S3) well supports our hypothesis.

The results obtained also reveals that the VS-model can be used for describing the processes underlying the environmental impact on the intra-annual tree-ring structure, at least within contexts characterized by climatic factors strong limiting growth, as at our site. In particular, the strength of the association between the simulated growth rates and the measured radial tracheid sizes supports the model assumption that tracheid radial size is pre-determined during the early stage of cell differentiation and can therefore be associated with the rate of cambial cells production (Vaganov *et al.*, 2006; Vaganov *et al.*, 2011). The climatic conditions occurring during this phase pre-determine the duration and rate that the forming cells are going to endure in the enlargement phase, which control the final tracheid size (Cuny *et al.*, 2014). Studies on correlation between tracheid size and environmental conditions have indeed often identified seasonal climatic signals overlaying the developmental phases of cambial division and tracheid enlargement, thus supporting the existence of

329 a strong association between them (e.g.; Fonti *et al.*, 2013; Carrer *et al.*, 2017; Castagneri *et al.*,
330 2017).

331 In this study we applied the model to assess which conditions (intensity and pattern of precipitation)
332 generate a latewood IADF in "an average tree" at the study site. Such an approach has a great
333 potential for exploring how climate is affecting wood formation, even at individual tree level. For
334 example it might be interesting to investigate what summer drought conditions are inducing a stop in
335 growth while considering both the level of drought and the individual tree growth potential by
336 performing similar analyses on trees and calendar years grouped according to ring width and/or tree
337 vigor.

338 ## 5 Conclusion

339 This study demonstrated that the VS-model successfully generated realistic tracheidograms of
340 tracheid cell diameter for *Pinus sylvestris* trees growing in a drought sensitive environment. In
341 particular the strong association between the growth rate of the dividing cambial cell and the tracheid
342 size was used to predict wood structure from daily climatic condition This intra-ring resolution has
343 been achieved thanks to the model ability to provide daily growth rates (Vaganov *et al.*, 2006). This
344 increased resolution helped us to identify narrow rings as an extreme manifestation of IADFs where
345 the recover in the second part of the season was impeded by a too high sensitivity to extreme drought
346 conditions. The model proved usefulness also to quantify average levels and seasonal patterns of
347 precipitation (thus indirectly of drought) inducing IADFs and narrow rings. The association between
348 climatic conditions and cell anatomical structure via model-generated tracheidogram provide a novel
349 opportunity to assess wood structure sensitivity to climate. Such intra-annual growth model
350 resolution represents a fundamental tool to provide reliable tracheidogram to better understand,
351 develop and up-scale scenarios of wood structural responses to climate change over time and space.
352 Considering that wood structure is an important legacy for tree performance (Björklund *et al.*, 2017;
353 Rathgeber, 2017) the results from those scenarios might have relevant implications for the
354 assessment of future plant productivity and provided forest services (Sass-Klaassen *et al.*, 2016).

355

356 ## 6 Author Contributions

357 M.P, E.V, V.S. and P.F. designed the research. E.B and M.F. performed data collection. M.P, M.F,
358 and P.F. performed analyses and interpreted the data. All coauthors contributed to the preparation of
359 the manuscript.

360

361 ## 7 Funding

362 The work has been supported by the Russian Science Foundation (project #14-14-00219 P for
363 simulation approach), the Le Studium/Marie Sklodowska-Curie research fellowship (for VS-
364 modeling), the State assignment "Science of Future" (project #5.3508.2017/4.6 for data analysis), the
365 Swiss National Science Foundation project LOTFOR (no. 150205), and the Russian Foundation for
366 Basic Research (project #17-04-00315 for sampling and measurements; and project #17-04-00610
367 for xylogenesis sampling and data).

368

8 Acknowledgments

The authors would like to thank Tatiana Kostyakova, Irina Sviderskaya, Ivan Tychkov for support, comments and suggestions, and Georg von Arx for a friendly review on the last version of the manuscript.

9 References

Abrantes, J., Campelo, F., Garcia-Gonzalez, I., and Nabais, C. (2013). Environmental control of vessel traits in Quercus ilex under Mediterranean climate: relating xylem anatomy to function. *Trees-Structure and Function* 27(3), 655-662. doi: 10.1007/s00468-012-0820-6.

Allen, C.D., Macalady, A.K., Chenchouni, H., Bachelet, D., McDowell, N., Vennetier, M., et al. (2010). A global overview of drought and heat-induced tree mortality reveals emerging climate change risks for forests. *Forest Ecology and Management* 259(4), 660-684. doi: DOI 10.1016/j.foreco.2009.09.001.

Anderegg, W., Plavcová, L., Anderegg, L.D.L., Hacke, U.G., Berry, J.A., and Field, C.B. (2013). Drought's legacy: multiyear hydraulic deterioration underlies widespread aspen forest die-off and portends increased future risk. *Global Change Biology* 19(4), 1188-1196. doi: 10.1111/gcb.12100.

Arzac, A., Babushkina, E., Slobodchikova, V., Fonti, P., Sviderskaya, I., and Vaganov, E. (in review). Evidences of increased carbon fixation in Pinus sylvestris tracheids in a forest-steppe of Southern Siberia. *Dendrochronologia*.

Babushkina, E.A., Vaganov, E.A., Belokopytova, L.V., Shishov, V.V., and Grachev, A.M. (2015). Competitive Strength Effect in the Climate Response of Scots Pine Radial Growth in South-Central Siberia Forest-Steppe. *Tree-Ring Research* 71(2), 106-117. doi: 10.3959/1536-1098-71.2.106.

Battipaglia, G., De Micco, V., Brand, W.A., Linke, P., Aronne, G., Saurer, M., et al. (2010). Variations of vessel diameter and delta 13C in false rings of Arbutus unedo L. reflect different environmental conditions. *New Phytologist* 188(4), 1099-1112. doi: 10.1111/j.1469-8137.2010.03443.x.

Björklund, J., Seftigen, K., Schweingruber, F., Fonti, P., von Arx, G., Bryukhanova, M.V., et al. (2017). Cell size and wall dimensions drive distinct variability of earlywood and latewood density in Northern Hemisphere conifers. *New Phytol* 216, 728–740. doi: 10.1111/nph.14639.

Breitenmoser, P., Bronnimann, S., and Frank, D. (2014). Forward modelling of tree-ring width and comparison with a global network of tree-ring chronologies. *Climate of the Past* 10(2), 437-449. doi: 10.5194/cp-10-437-2014.

Britez, M.R.D., Sergent, A.S., Meier, A.M., Breda, N., and Rozenberg, P. (2014). Wood density proxies of adaptive traits linked with resistance to drought in Douglas fir (Pseudotsuga menziesii (Mirb.) Franco). *Trees-Structure and Function* 28(5), 1289-1304. doi: 10.1007/s00468-014-1003-4.

Camarero, J.J., Olano, J.M., and Parras, A. (2010). Plastic bimodal xylogenesis in conifers from continental Mediterranean climates. *New Phytologist* 185(2), 471-480. doi: 10.1111/j.1469-8137.2009.03073.x.

Campelo, F., Nabais, C., Carvalho, A., and Vieira, J. (2016). tracheideR-An R package to standardize tracheidograms. *Dendrochronologia* 37, 64-68. doi: 10.1016/j.dendro.2015.12.006.

412 Campelo, F., Nabais, C., Freitas, H., and Gutierrez, E. (2007). Climatic significance of tree-ring
413 width and intra-annual density fluctuations in Pinus pinea from a dry Mediterranean area in
414 Portugal. *Annals of Forest Science* 64(2), 229-238. doi: 10.1051/forest:2006107.
415 Campelo, F., Vieira, J., Battipaglia, G., de Luis, M., Nabais, C., Freitas, H., et al. (2015). Which
416 matters most for the formation of intra-annual density fluctuations in Pinus pinaster: age or
417 size? *Trees-Structure and Function* 29(1), 237-245. doi: 10.1007/s00468-014-1108-9.
418 Campelo, F., Vieira, J., and Nabais, C. (2013). Tree-ring growth and intra-annual density fluctuations
419 of Pinus pinaster responses to climate: does size matter? *Trees-Structure and Function* 27(3),
420 763-772. doi: 10.1007/s00468-012-0831-3.
421 Carrer, M., Castagneri, D., Prendin, A.L., Petit, G., and von Arx, G. (2017). Retrospective Analysis
422 of Wood Anatomical Traits Reveals a Recent Extension in Tree Cambial Activity in Two
423 High-Elevation Conifers. *Frontiers in Plant Science* 8. doi: 10.3389/fpls.2017.00737.
424 Castagneri, D., Fonti, P., von Arx, G., and Carrer, M. (2017). How does climate influence xylem
425 morphogenesis over the growing season? Insights from long-term intra-ring anatomy in Picea
426 abies. *Annals of Botany* 119(6), 1011-1020. doi: 10.1093/aob/mcw274.
427 Castagneri, D., Petit, G., and Carrer, M. (2015). Divergent climate response on hydraulic-related
428 xylem anatomical traits of Picea abies along a 900-m altitudinal gradient. *Tree Physiology*
429 35(12), 1378-1387. doi: 10.1093/treephys/tpv085.
430 Cook, E., and Kairiukstis, L. (1990). *Methods of dendrochronology: applications in the*
431 *environmental science*. Dordrecht, Netherlands ; Boston: Kluwer Academic Publishers.
432 Cuny, H.E., Rathgeber, C.B.K., Frank, D., Fonti, P., and Fournier, M. (2014). Kinetics of tracheid
433 development explain conifer tree-ring structure. *New Phytologist* 203(4), 1231-1241. doi: Doi
434 10.1111/Nph.12871.
435 Cuny, H.E., Rathgeber, C.B.K., Frank, D., Fonti, P., Makinen, H., Prislan, P., et al. (2015). Woody
436 biomass production lags stem-girth increase by over one month in coniferous forests. *Nature*
437 *Plants* 1(11). doi: 10.1038/Nplants.2015.160.
438 Cuny, H.E., Rathgeber, C.B.K., Kiesse, T.S., Hartmann, F.P., Barbeito, I., and Fournier, M. (2013).
439 Generalized additive models reveal the intrinsic complexity of wood formation dynamics.
440 *Journal of Experimental Botany* 64(7), 1983-1994. doi: DOI 10.1093/jxb/ert057.
441 De Micco, V., Campelo, F., De Luis, M., Brauning, A., Grabner, M., Battipaglia, G., et al. (2016).
442 Intra-Annual Density Fluctuations in Tree Rings: How, When, Where, and Why? *Iawa*
443 *Journal* 37(2), 232-259. doi: 10.1163/22941932-20160132.
444 Deleuze, C., and Houllier, F. (1998). A simple process-based xylem growth model for describing
445 wood microdensitometric profiles. *Journal of Theoretical Biology* 193(1), 99-113. doi: DOI
446 10.1006/jtbi.1998.0689.
447 Delpierre, N., Soudani, K., Francois, C., Le Maire, G., Bernhofer, C., Kutsch, W., et al. (2012).
448 Quantifying the influence of climate and biological drivers on the interannual variability of
449 carbon exchanges in European forests through process-based modelling. *Agricultural and*
450 *Forest Meteorology* 154, 99-112. doi: 10.1016/j.agrformet.2011.10.010.
451 Downes, G.M., Drew, D., Battaglia, M., and Schulze, D. (2009). Measuring and modelling stem
452 growth and wood formation: An overview. *Dendrochronologia* 27(2), 147-157. doi:
453 10.1016/j.dendro.2009.06.006.
454 Eilmann, B., Zweifel, R., Buchmann, N., Fonti, P., and Rigling, A. (2009). Drought-induced
455 adaptation of the xylem in Scots pine and pubescent oak. *Tree Physiology* 29(8), 1011-1020.
456 doi: Doi 10.1093/Treephys/Tpp035.
457 Fonti, P., Bryukhanova, M.V., Myglan, V.S., Kirdyanov, A.V., Naumova, O.V., and Vaganov, E.A.
458 (2013). Temperature-induced responses of xylem structure of Larix sibirica (pinaceae) from
459 the Russian Altay. *American Journal of Botany* 100(7), 1332-1343. doi:
460 10.3732/ajb.1200484.

Fonti, P., von Arx, G., Garcia-Gonzalez, I., Eilmann, B., Sass-Klaassen, U., Gartner, H., et al. (2010). Studying global change through investigation of the plastic responses of xylem anatomy in tree rings. *New Phytologist* 185(1), 42-53. doi: Doi 10.1111/J.1469-8137.2009.03030.X.

Fritts, H.C. (1976). *Tree rings and climate*. London ; New York: Academic Press.

Grissino-Mayer, H.D. (2001). Evaluating Crossdating Accuracy: A Manual and Tutorial for the Computer Program COFECHA. *Tree-Ring Research* 57(2), 205-221.

Guiot, J., Boucher, E., and Gea-Izquierdo, G. (2014). Process models and model-data fusion in dendroecology. *Frontiers in Ecology and Evolution* 2(52). doi: 10.3389/fevo.2014.00052.

He, M., Shishov, V., Kaparova, N., Yang, B., Brauning, A., and Griessinger, J. (2017). Process-based modeling of tree-ring formation and its relationships with climate on the Tibetan Plateau. *Dendrochronologia* 42, 31-41. doi: 10.1016/j.dendro.2017.01.002.

Martin-Benito, D., Anchukaitis, K.J., Evans, M.N., del Rio, M., Beeckman, H., and Canellas, I. (2017). Effects of Drought on Xylem Anatomy and Water-Use Efficiency of Two Co-Occurring Pine Species. *Forests* 8(9). doi: 10.3390/f8090332.

Mayr, S., Bardage, S., and Brandstrom, J. (2006). Hydraulic and anatomical properties of light bands in Norway spruce compression wood. *Tree Physiology* 26(1), 17-23.

McCarroll, D., and Loader, N.J. (2004). Stable isotopes in tree rings. *Quaternary Science Reviews* 23(7-8), 771-801. doi: 10.1016/j.quascirev.2003.06.017.

McDowell, N., Pockman, W.T., Allen, C.D., Breshears, D.D., Cobb, N., Kolb, T., et al. (2008). Mechanisms of plant survival and mortality during drought: why do some plants survive while others succumb to drought? *New Phytologist* 178(4), 719-739. doi: DOI 10.1111/j.1469-8137.2008.02436.x.

Meinzer, F.C., Lachenbruch, B., and Dawson, T.E. (2011). "Size-and age-related changes in tree structure and function", in: *Tree physiology,*. (Dordrecht Netherlands ; New York: Springer,).

Nabais, C., Campelo, F., Vieira, J., and Cherubini, P. (2014). Climatic signals of tree-ring width and intra-annual density fluctuations in Pinus pinaster and Pinus pinea along a latitudinal gradient in Portugal. *Forestry* 87(4), 598-605. doi: 10.1093/forestry/cpu021.

Ogee, J., Brunet, Y., Loustau, D., Berbigier, P., and Delzon, S. (2003). MuSICA, a CO2, water and energy multilayer, multileaf pine forest model: evaluation from hourly to yearly time scales and sensitivity analysis. *Global Change Biology* 9(5), 697-717. doi: DOI 10.1046/j.1365-2486.2003.00628.x.

Olivar, J., Bogino, S., Spiecker, H., and Bravo, F. (2015). Changes in climate-growth relationships and IADF formation over time of pine species (Pinus halepensis, P-pinaster and P-sylvestris) in Mediterranean environments. *Forest Systems* 24(1). doi: 10.5424/fs/2015241-05885.

Pacheco, A., Camarero, J.J., and Carrer, M. (2016). Linking wood anatomy and xylogenesis allows pinpointing of climate and drought influences on growth of coexisting conifers in continental Mediterranean climate. *Tree Physiology* 36(4), 502-512. doi: 10.1093/treephys/tpv125.

Pasho, E., Camarero, J.J., and Vicente-Serrano, S.M. (2012). Climatic impacts and drought control of radial growth and seasonal wood formation in Pinus halepensis. *Trees-Structure and Function* 26(6), 1875-1886. doi: 10.1007/s00468-012-0756-x.

Rathgeber, C.B.K. (2017). Conifer tree-ring density inter-annual variability – anatomical, physiological and environmental determinants. *New Phytologist* 216(3), 621-625. doi: 10.1111/nph.14763.

Rathgeber, C.B.K., Cuny, H.E., and Fonti, P. (2016). Biological basis of tree-ring formation: A crash course. *Frontiers in Plant Science* 7(MAY2016). doi: 10.3389/fpls.2016.00734.

Rigling, A., Waldner, P.O., Forster, T., BraSker, O.U., and Pouttu, A. (2001). Ecological interpretation of tree-ring width and intraannual density fluctuations in Pinus sylvestris on dry sites in the central Alps and Siberia. *Canadian Journal of Forest Research-Revue Canadienne De Recherche Forestiere* 31(1), 18-31. doi: DOI 10.1139/cjfr-31-1-18.

Rossi, S., Anfodillo, T., Cufar, K., Cuny, H.E., Deslauriers, A., Fonti, P., et al. (2016). Pattern of xylem phenology in conifers of cold ecosystems at the Northern Hemisphere. *Global Change Biology* 22(11), 3804-3813. doi: 10.1111/gcb.13317.

Sass-Klaassen, U., Fonti, P., Cherubini, P., Gričar, J., Robert, E.M.R., Steppe, K., et al. (2016). A tree-centered approach to assess impacts of extreme climatic events on forests. *Frontiers in Plant Science* 7, 1069. doi: 10.3389/fpls.2016.01069.

Schiestl-Aalto, P., Kulmala, L., Makinen, H., Nikinmaa, E., and Makela, A. (2015). CASSIA - a dynamic model for predicting intra-annual sink demand and interannual growth variation in Scots pine. *New Phytologist* 206(2), 647-659. doi: 10.1111/nph.13275.

Seo, J.W., Smiljanic, M., and Wilmking, M. (2014). Optimizing cell-anatomical chronologies of Scots pine by stepwise increasing the number of radial tracheid rows included-Case study based on three Scandinavian sites. *Dendrochronologia* 32(3), 205-209. doi: Doi 10.1016/J.Dendro.2014.02.002.

Shi, S.L., Li, Z.S., Wang, H., von Arx, G., Lu, Y.H., Wu, X., et al. (2016). Roots of forbs sense climate fluctuations in the semi-arid Loess Plateau: Herb-chronology based analysis. *Scientific Reports* 6. doi: 10.1038/srep28435.

Shishov, V.V., Tychkov, I.I., Popkova, M.I., Ilyin, V.A., Bryukhanova, M.V., and Kirdyanov, A.V. (2016). VS-oscilloscope: A new tool to parameterize tree radial growth based on climate conditions. *Dendrochronologia* 39, 42-50. doi: 10.1016/j.dendro.2015.10.001.

Silkin, P.P. (2010). *Methods of multiparameter analysis of conifers tree-rings structure.* Krasnoyarsk Siberian Federal University.

Steppe, K., Sterck, F., and Deslauriers, A. (2015). Diel growth dynamics in tree stems: linking anatomy and ecophysiology. *Trends in Plant Science* 20(6), 335-343. doi: 10.1016/j.tplants.2015.03.015.

Touchan, R., Shishov, V.V., Meko, D.M., Nouiri, I., and Grachev, A. (2012). Process based model sheds light on climate sensitivity of Mediterranean tree-ring width. *Biogeosciences* 9(3), 965-972. doi: 10.5194/bg-9-965-2012.

Tychkov, I., Shishov, V., Sviderskaya, I., Babushkina, E., Popkova, M., and Vaganov, E. (in review). How parameterization of process-based model can help us to understand real tree-ring growth.

Vaganov, E. (1990). "The tracheidogram method in tree-ring analysis and its application," in *Methods of dendrochronology: applications in the environmental sciences,* eds. E. Cook & L. Kairiukstis. (Dordrecht, The Netherlands: Kluwer Academic), 63–76.

Vaganov, E., Anchukaitis, K., and Evans, M. (2011). "How Well Understood Are the Processes that Create Dendroclimatic Records? A Mechanistic Model of the Climatic Control on Conifer Tree-Ring Growth Dynamics," in *Dendroclimatology: Progress and Prospects,* eds. M. Hughes, T. Swetnam & H. Diaz. Dordrecht: Springer,), 37-75.

Vaganov, E., Shashkin, A., Sviderskaya, I., and Vysotskaya, L. (1985). *Histometric Analysis of Woody Plant Growth.*

Vaganov, E.A., Hughes, M.K., and Shashkin, A.V. (2006). *Growth Dynamics of Conifer Tree Rings: Images of Past and Future Environments.* Springer.

Vieira, J., Campelo, F., and Nabais, C. (2009). Age-dependent responses of tree-ring growth and intra-annual density fluctuations of Pinus pinaster to Mediterranean climate. *Trees-Structure and Function* 23(2), 257-265. doi: 10.1007/s00468-008-0273-0.

Vieira, J., Nabais, C., Rossi, S., Carvalho, A., Freitas, H., and Campelo, F. (2017). Rain exclusion affects cambial activity in adult maritime pines. *Agricultural and Forest Meteorology* 237, 303-310. doi: 10.1016/j.agrformet.2017.02.024.

Vieira, J., Rossi, S., Campelo, F., Freitas, H., and Nabais, C. (2014). Xylogenesis of Pinus pinaster under a Mediterranean climate. *Annals of Forest Science* 71(1), 71-80. doi: DOI 10.1007/s13595-013-0341-5.

Wilkinson, S., Ogee, J., Domec, J.C., Rayment, M., and Wingate, L. (2015). Biophysical modelling of intra-ring variations in tracheid features and wood density of Pinus pinaster trees exposed to seasonal droughts. *Tree Physiology* 35(3), 305-318. doi: 10.1093/treephys/tpv010.

Yang, B., He, M.H., Shishov, V., Tychkov, I., Vaganov, E., Rossi, S., et al. (2017). New perspective on spring vegetation phenology and global climate change based on Tibetan Plateau tree-ring data. *Proceedings of the National Academy of Sciences of the United States of America* 114(27), 6966-6971. doi: 10.1073/pnas.1616608114.

Zalloni, E., de Luis, M., Campelo, F., Novak, K., De Micco, V., Di Filippo, A., et al. (2016). Climatic Signals from Infra-annual Density Fluctuation Frequency in Mediterranean Pines at a Regional Scale. *Frontiers in Plant Science* 7. doi: 10.3389/fpls.2016.00579.

Zhang, J.Z., Gou, X.H., Zhang, Y.X., Lu, M., Xu, X.Y., Zhang, F., et al. (2016). Forward modeling analyses of Qilian Juniper (Sabina przewalskii) growth in response to climate factors in different regions of the Qilian Mountains, northwestern China. *Trees-Structure and Function* 30(1), 175-188. doi: 10.1007/s00468-015-1286-0.

10 Figures

Figure 1. Model calibration and selection of ring types. (A) The grey line indicates the detrended Pinus sylvestris tree-ring chronology over the period 1936 to 2013 at the Malaya Minusa in southern Siberia; the black one shows the growth rate obtained with the model. Pearson's correlations (r) and Gleichläufigkeit (Glk) for both the calibration (1960-2013) and verification period (1936-1959) are indicated. Colored years indicate the annual rings grouping (N = narrow rings (green); W = wide rings (blue); I = IADF rings (red)) according to their typical tree-ring pattern. **(B)** Images of a ring displaying a typical IADF (ring 2013, scale = 100 μm).

Figure 2. Tracheidograms and intra-annual density fluctuations (IADF). (A) Overview of all 50 tracheidograms of tracheid diameter for the annual rings of tree D8 with different ring types shown in colors (N = narrow rings (green); W = wide rings (blue); I = IADF rings (red), see Figure 1 and Figure 2B). **(B)** Example of tracheidogram displaying a L+ IADF (numbers indicate the tracheid diameter). L+ IADFs have been defined in this study as rings showing a tracheid size increase of at least 10% occurring in the last third of the tracheidogram. The formula in red indicates how the increase of tracheid diameter (DeltaIADF) has been assessed. **(C)** Presence of DeltaIADFs as a function of tree-ring width for all the 250 annual rings considered in the study. In black are indicated the years of the annual ring showing a L+ IADF (i.e. with DeltaIADF >10%). The year in red corresponds to the example of Figure 2B.

Figure 3. Assessment of cambial cell growth rates and its relationship to the tracheid diameter. (A) Average number of cambial (beige) and enlarging cells (yellow) as observed during the growing season 2013 with repeated micro-coring on 15 trees from the study site in Malaya Minusa. **(B)** Daily (grey bars) and cumulated (black thick line) growth rates as assessed by the calibrated model for the growing season 2013. Brown rectangles on the right indicate the sequentially developing cambial cells (n=31 for tree D1, assuming that the production of a successive cambium cell only occurs when the previous one is completed) used to assess the timing of their development and the corresponding average cell growth rate (the filled rectangle correspond to the 21st cambial cell). Specifically, the timing of each dividing cambial cell (i.e., when environmental conditions determine the future cell

604 differentiation, see (Vaganov et al., 2006)) was assigned by dividing the annual Gr by the number of
605 cells produced. **(C)** Correlation between average cell growth rate and tracheid diameter for the
606 example shown in Figure 3B (year 2013 of tree D1, numbers indicate the cell position in the ring);
607 and **(D)** scatter plot of average cell growth rate and tracheid diameter for all 9468 tracheids included
608 in the 250 tracheidograms. The exponential fitting function is shown in red. **(E)** Summary of all
609 correlations between average cell growth rate (Gr) and tracheid diameter (TD) plotted as a function
610 of ring width (n=250). The red dot refers to the example shown in Figure 3C. The red line shows the
611 distribution of the correlations.
612
613 **Figure 4. Comparison of climate, growth rate, and modeled wood structure among the three**
614 **ring types (narrow rings (green); wide rings (blue); IADF rings (red))**. **(A)** Daily temperature
615 (dots) and precipitation (area) averaged for each the year in each ring type and smoothed with a loess
616 function (span=0.3, thick lines). The smoothed values have been used as input for the model. **(B)**
617 Growth rates obtained by the model. **(C)** Derived tracheidogram for each ring type by using the
618 quantified relation between average cell growth rates and tracheid diameter (Figure 3D). The number
619 of cell is proportional to the modeled ring width. **(D)** Schema of the tracheidogram shown in **(C)**.
620
621 **Figure 5. Exploring climatic scenarios generating IADF**. **(A)** Averaged and loess smoothed
622 (span=0.3) daily precipitation of each ring type (thick colored lines) and their progressive transition
623 between groups (in 20% steps) between W - I and I -N (thin grey lines) used to run the model (with
624 group average daily temperature). The black line indicates the average precipitation over the period
625 1960 to 2013. Psum [mm] Doy 0-186 = precipitation sum between DOY 1 and 186 (middle of the
626 growing season); Psum [mm] Doy187-276 = precipitation sum between DOY 187 and 276 (end of
627 the growing season). **(B)** Obtained daily growth rates. The legend quantifies the growth rates sum
628 [%] for each climatic scenario. **(C)** Derived modeled tracheidograms for each precipitation scenario.
629 Tracheidograms with filled circle display a L+ IADF according to the definition given in Figure 2B.
630 The legend quantifies the DeltaIADF [%] for each climatic scenario. N = narrow rings (green); W =
631 wide rings (blue); I = IADF rings (red).

TABLES AND FIGURES

Table 1: **Trees and tree-ring characteristics.**

	H	DBH	Age	TRW			Ncell			TD		
	[m]	[cm]	[years]	[mm]						[µm]		
	mean	mean	mean	mean	min	max	mean	min	max	mean	min	max
All 20 trees	**17.8**	**37.5**	93	**1.46**	0.59	3.22	-	-	-	-	-	-
Five trees	**18.2**	**35.8**	**95**	**1.33**	0.22	2.88	**38**	9	76	**35.0**	**18.7**	**45.5**
Tree1	**18**	**40**	**90**	**1.75**	1.05	2.88	**44**	29	71	**40.2**	36.2	45.5
Tree2	**17**	**26**	**91**	**1,69**	0.69	2.64	**49**	23	76	**33.9**	29.0	37.2
Tree5	**20**	**41**	**90**	**0.73**	0.22	2.51	**21**	9	70	**33.4**	18.7	38.9
Tree7	**20**	**43**	**111**	**1.27**	0.57	2.38	**43**	23	73	**29.0**	23.1	33.7
Tree8	**16**	**29**	**92**	**1.22**	0.51	1.99	**32**	17	53	**38.4**	28.5	44.8
15 trees 9.1 monitored	**9.2**	**9.3**	**9.4**	**3 9.5 6**	: 9.6	9.7	**9.8**	- 9.9	9.10	**9.11**	9.12	-

H = Tree height; DBH = Stem diameter at breast height; TRW = tree-ring width; Ncell = number of cells in tracheidogram; TD = Cross-sectional tracheid radial diameter

Table 2: **Selected model parameters**

Param	Description	Values
T_{min}	Minimum temperature threshold for growth (°C)	5.0
T_{opt1}	Lower temperatures threshold for optimal growth (°C)	13.0
T_{opt2}	Upper temperatures threshold for optimal growth (°C)	22.0
T_{max}	Maximum temperature threshold for growth (°C)	32.0
W_{min}	Minimum soil moisture threshold for growth, relative to saturated soil (v/v)	0.0775
W_{opt1}	Lower soil moistures threshold for optimal growth (v/v)	0.25
W_{opt2}	Upper soil moistures threshold for optimal growth (v/v)	0.375
W_{max}	Maximum soil moisture threshold for growth (v/v)	0.45
W_0	Initial soil moisture (v/v)	0.15
T_{beg}	Temperature sum threshold for onset of growth (°C)	110.0
t_{beg}	Size of the moving window for calculation of temperature sum (days)	10
l_r	Depth of root system (mm)	500
P_{max}	Maximum daily precipitation for saturated soil (mm/day)	40
C_1	Fraction of precipitation reaching the soil (not caught by crown) (rel. unit)	0.5
C_2	First coefficient for calculation of transpiration (mm/day)	0.3075
C_3	Second coefficient for calculation of transpiration (mm/day)	0.11
Λ	Coefficient for water drainage from soil (rel. unit)	0.005
V_{cr}	Critical growth rate to determine the end of the growing season (rel. unit)	0.04

Figure 1.JPEG

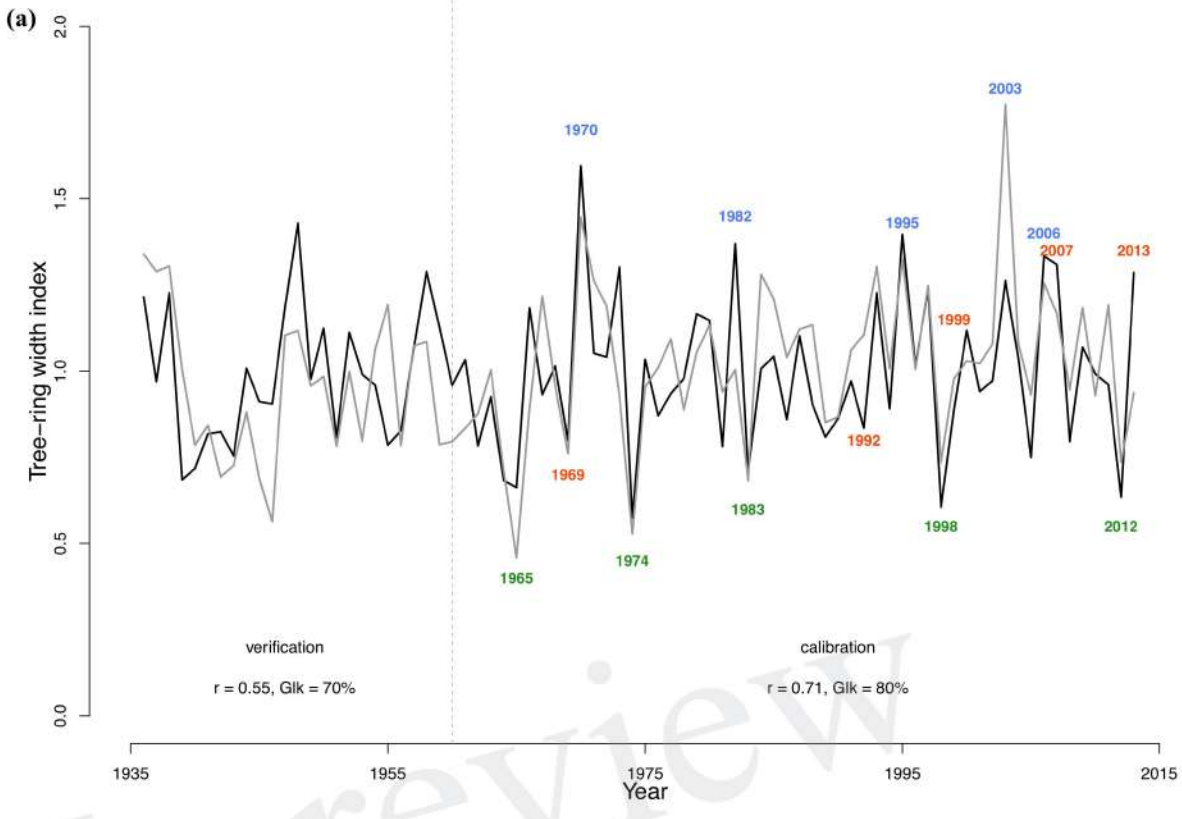

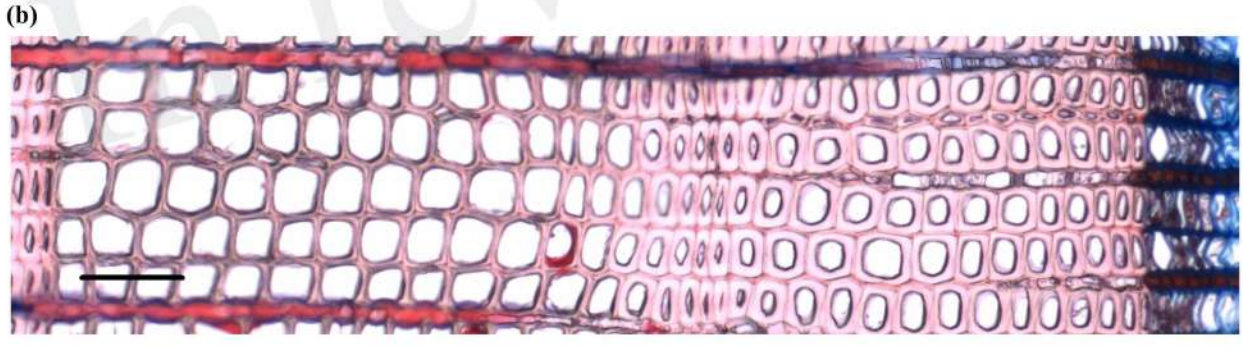

Figure 2.JPEG

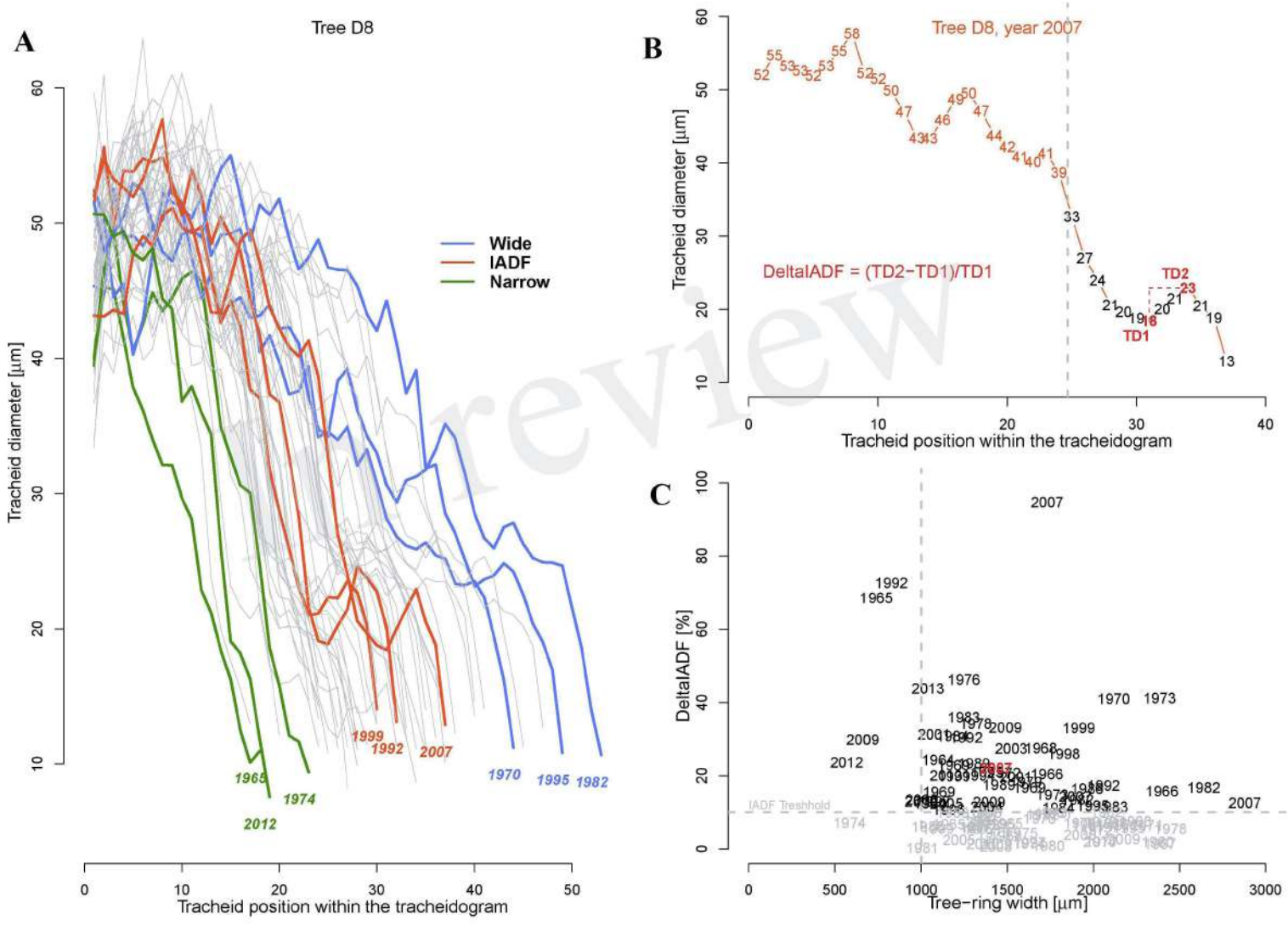

Figure 3.JPEG

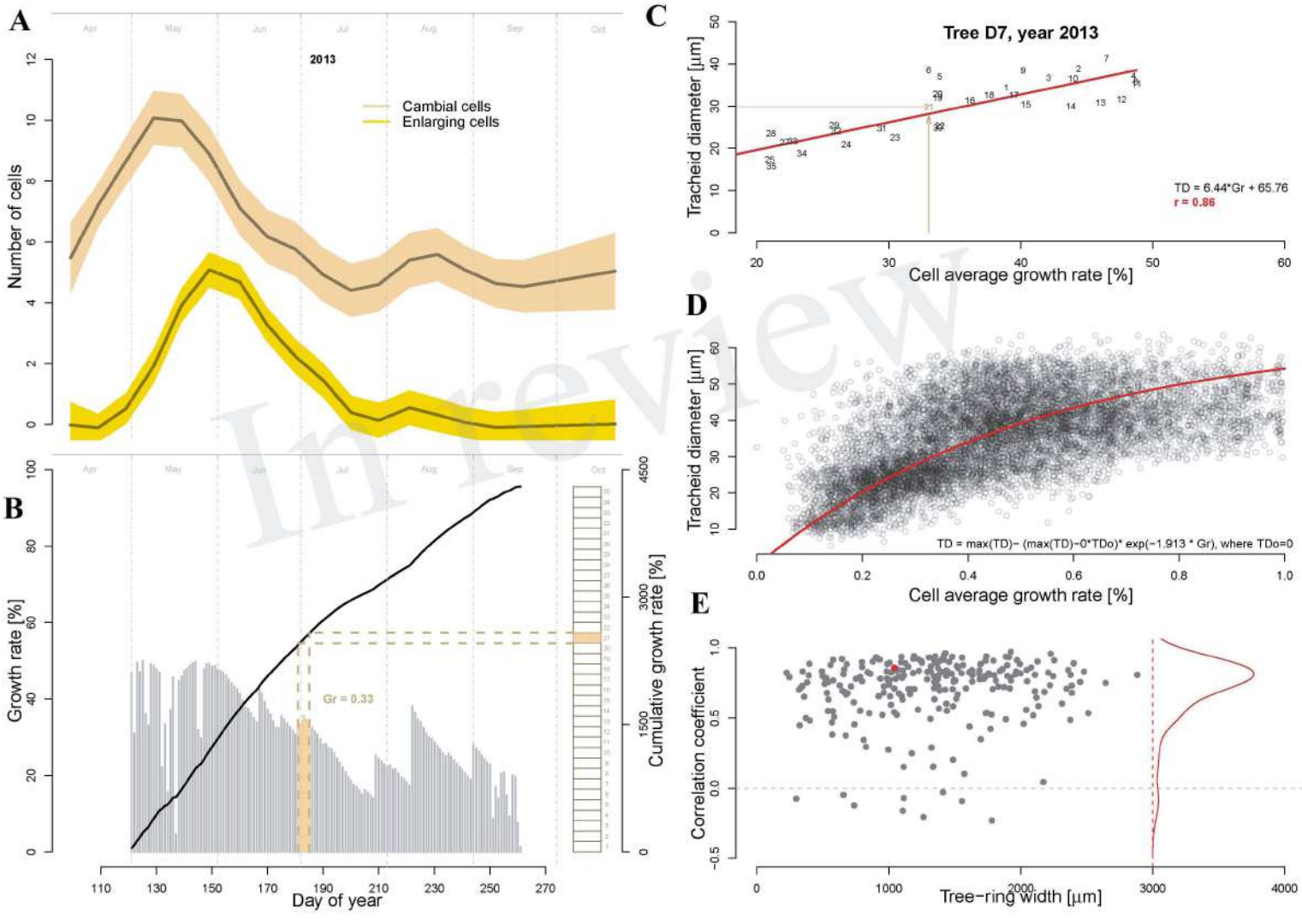

Figure 4.JPEG

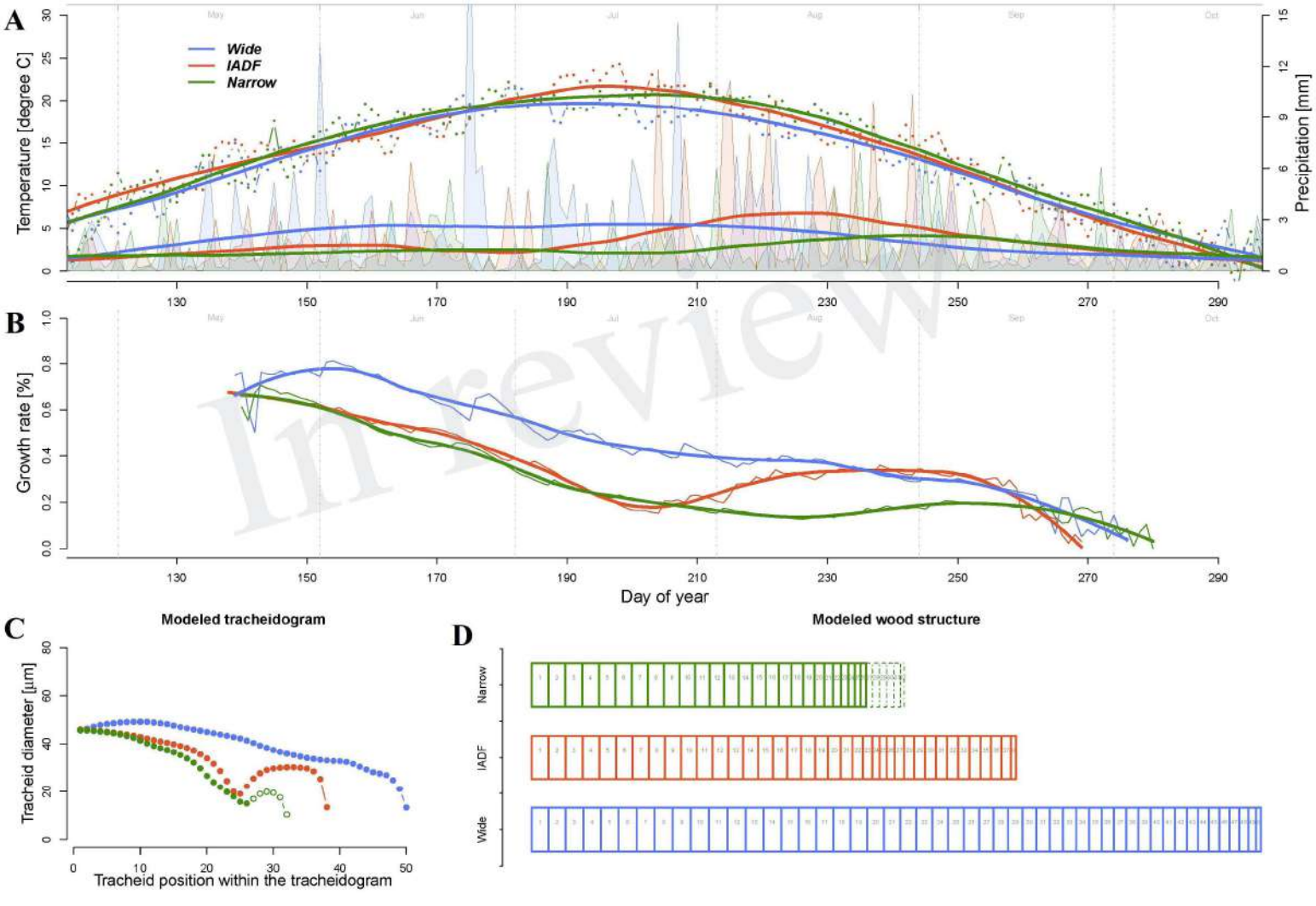

Figure 5.JPEG